J Electroceram (2010) 24:261–269
DOI 10.1007/s10832-009-9567-x

The electronic conductivity of $Ba_{0.5}Sr_{0.5}Co_xFe_{1-x}O_{3-\delta}$ (BSCF: x=0~1.0) under different oxygen partial pressures

Jae-Il Jung · Scott T. Misture · Doreen D. Edwards

Received: 16 May 2008 / Accepted: 4 March 2009 / Published online: 1 April 2009

Abstract The electronic conductivity of sintered BSCF ceramics ($Ba_{0.5}Sr_{0.5}Co_xFe_{1-x}O_{3-\delta}$, $0 \le x \le 1$) was measured as a function of temperature up to 1273 K in air. The conductivity of BSC is thermally activated over 298–1273 K with an activation energy of 0.21 eV. The conductivity of BSF and BSCF ($0.2 \le x \le 0.8$) is thermally activated below ~673 K with activation energies of 0.21 eV–0.40 eV. Above 673 K, the formation of oxygen vacancies results in a decrease in p-type carrier concentration and a decrease in electronic conductivity. $Ba_{0.5}Sr_{0.5}Co_{0.8}Fe_{0.2}O_{3-\delta}$ (BSCF5582) was also measured under 10^{-5} atm$\le pO_2 \le 1$ atm. Below ~673 K, the electronic conductivity of BSCF 5582 shows no dependence on pO_2. Above 673 K, the conductivity of BSCF5582 increases with increasing pO_2 for $pO_2 \ge 0.01$ (p-type conduction) and decreases slightly with increasing pO_2 for $pO_2 \le 0.01$ atm. The activation energy for conduction above ~673 K and at $pO_2 \ge 0.1$ is ~0.07 eV. Above ~823K and at $pO_2 \ge 0.01$ atm, the activation energy for conduction is ~0.2 eV.

Keywords BSCF · Barium strontium cobalt iron oxide · Perovskite · Solid oxide fuel cell · Cathode · Mixed ionic-electronic conductor · Defect chemistry

1 Introduction

The perovskite $Ba_{0.5}Sr_{0.5}Co_{0.8}Fe_{0.2}O_{3-\delta}$ (BSCF5582) has attracted considerable attention as a promising cathode material for intermediate temperature solid oxide fuel cells (IT-SOFC) since Shao and Haile reported on its performance in dual and single chamber fuel cells in 2004 [1]. Initially developed as an oxygen separation membrane [2], BSCF is a mixed ionic electronic conductor (MIEC) deriving its high oxygen ion conductivity from its oxygen-deficient perovskite structure. The oxygen nonstoichiometry of BSCF5582 has been measured by several researchers with the reported values of δ ranging from ~0.2 to 0.8 depending on temperature, oxygen partial pressure, and method of measurement [3–6]. Chen et al. [7] reported room-temperature δ values ranging from 0.17 to 0.32 for BSCF with varying Co:Fe ratios. Bucher et al. reported the oxygen self-diffusion coefficient and ionic conductivity of BSCF5582 at 700°C to be on the order of 10^{-6} cm^2/s and 0.018 S/cm, respectively [6].

BSCF exhibits moderately high electronic conductivity owing to the mixed valence of the transition metal B-site cations. As an example, the electrical conductivity of BSCF5582 in air above 500°C is reported to be ~30 S/cm [8]. However, the conductivity of BSCF5582 is over an order of magnitude lower than $La_{0.8}Sr_{0.2}Co_{0.8}Fe_{0.2}O_3$ (or LSCF), a related perovskite oxide used as a SOFC cathode [9]. Unlike LSCF, BSCF does not possess a trivalent cation on the A site of the perovskite structure.

The defect chemistry of $Ba_ySr_{1-y}Co_xFe_{1-x}O_{3-\delta}$ (BSCF) is not well understood as there have been few reports on the effect of composition and oxygen partial pressure on its electrical conductivity. Grunbaum et al. investigated the electrical conductivity of $SrCo_{0.8}Fe_{0.2}O_{3-\delta}$ as a function of temperature and pO_2, reporting an activation energy of 0.17 eV for the Brownmillerite phase below 1000 K and of ~0.34 eV for the cubic phase above 1000 K [10]. In an investigation of compositions with x=0.8, $0.3 \le y \le 0.7$, Wei et al. showed that conductivity decreases with increasing barium content in air at 773–1023 K [11]. Chen et al.

J.-I. Jung · S. T. Misture · D. D. Edwards (✉)
Kazuo Inamori School of Engineering, Alfred University,
Alfred, NY 14802, USA
e-mail: dedwards@alfred.edu

showed an increase in conductivity with increasing cobalt concentration in air and in oxygen above 773 K for samples with y=0.5, 0≤x≤0.8 [7]. More recently, Ge et al. and Zhou et al. investigated the effects of A-site and B-site deficiencies on electrical conductivity [12–14]. In general, the electrical conductivity decreases as the ratio of A/B deviates from unity.

This work focuses on the effect of different Fe/Co ratios on the electrical conductivity of $Ba_{0.5}Sr_{0.5}Co_xFe_{1-x}O_{3-\delta}$ (0≤x≤1) in air. The electrical conductivity of polycrystalline $Ba_{0.5}Sr_{0.5}Co_xFe_{1-x}O_{3-\delta}$ (0≤x≤1.0) was measured as a function of temperature (25–1000°C) in air and correlated to thermal expansion and weight loss behavior reported previously by our group [15]. The conductivity of BSCF5582 was also measured as a function of temperature under different oxygen partial pressures, 10^{-5}≤pO_2≥1 atm. The defect chemistry responsible for the observed behavior is discussed.

2 Experimental methods

$Ba_{0.5}Sr_{0.5}Co_{1-x}Fe_xO_{3-\delta}$ powders were prepared using a polymerized complex method reported previously [15,16] The starting materials consist of barium nitrate ($Ba(NO_3)_2$, ≥99.0% purity, Alfa Aesar Co.), strontium nitrate ($Sr(NO_3)_2$, ≥99.0% purity, Aldrich Chemical Co.), cobalt(II) nitrate ($Co(NO_3)_2{\cdot}6H_2O$, ≥99.0% purity, Alfa Aesar Co.), and iron (III) nitrate ($Fe(NO_3)_3{\cdot}9H_2O$, ≥98.0% purity, Alfa Aesar Co.). A 0.04 mole quantity of ethylenediamine tetraacetic acid (EDTA) was mixed with 40 ml of 1N NH_4OH solution to make an NH_4-EDTA buffer solution. Equal molar amounts of barium nitrate and strontium nitrate (0.01 mol each) and appropriate amounts of $Co(NO_3)_2{\cdot}6H_2O$ and Fe $(NO_3)_3{\cdot}9H_2O$ were added to the buffer solution to make the required stoichiometries of $Ba_{0.5}Sr_{0.5}Co_xFe_{1-x}O_{3-\delta}$ (x=0.0, 0.2, 0.4, 0.6, 0.8, 1.0). Anhydrous citric acid (0.06 mol) was added, and the pH value was adjusted to 8 by using 1N NH_4OH solution. Each solution was kept on a hot plate at 100°C and stirred until gelation occurred. After 24 h, the gelled samples were baked in a drying oven at 200°C for 6 h. The as-produced powders were then calcined at 950°C for 7 h in air.

The synthesized powders were pressed into pellets at 100 MPa. The samples were sintered at 1100°C for 4 h in air at a heating rate of 4°C/min. The relative bulk density of each sample was measured using Archimedes' method. The crystal structure and phase purity of the synthesized powders were confirmed using X-ray diffraction, using a Siemens D5000 diffractometer using Cu-Kα radiation, a scan range of 15° to 80°, a step size of 0.02°, and a counting time of 5 s. Lattice parameters were determined using a least-squares method.

Sintered pellets were cut into rectangular shapes of 2 mm×3 mm×4 mm (a×b×L). Two small grooves (0.01" in diameter) were cut into the sample surface at 1/4 and 3/4 of the length (L) of the bars to prevent slippage of the inner platinum wires connected to the volt meter. Platinum ink (6082, BASF Catalysts, Newark, NJ) was painted on the cross-sectional faces of the sample to form current electrodes. The painted samples were heated at 900°C for 15 min to cure the electrodes. The electrical conductivity was measured using the four-point DC method, using ~100 mA of current passing through the outer electrodes and measuring the voltage drop across the inner electrodes. The measurements were performed isothermally in air and in various argon/oxygen mixtures upon heating from 200 to 1000°C using steps of 100°C. At each temperature step, 10 min was allowed for the conductivity stabilization. Conductivity, σ, was calculated as,

$$\sigma = \frac{I}{V}\frac{\ell}{A}, \tag{1}$$

where, I is current (~100 mA), V is voltage drop, l is the inner electrode spacing, and A (a×b) is the cross-sectional area of the bar.

Electrical conductivity was measured using a Labview controlled system consisting of a current source (Model JQE 55–2M, Kepco Power Supply, USA), a voltage meter (Model 2000 Digital Multimeter, Keithley Instruments, USA), a current meter (Model 2000 Digital Multimeter, Keithley Instruments, USA), and a furnace (Model Ney Centurion Qex, USA). Oxygen partial pressures were measured using an oxygen analyzer (Model Thermox CG1000, AMETEK, USA) on the outlet of furnace chamber.

3 Results

Figure 1 shows the X-ray diffraction patterns across the compositional range. BSF ($Ba_{0.5}Sr_{0.5}FeO_{3-\delta}$) and BSCF (0.2≤$x$≤0.8) are cubic perovskites, whereas BSC ($Ba_{0.5}Sr_{0.5}CoO_{3-\delta}$) has a rhombohedral structure. With increasing cobalt concentration, there is an increase in the unit cell volume of the material, shown by the shift of 2θ to lower angles in Fig. 1. A comparison of the ionic radii of iron and cobalt in different valences (r_{Fe4+}=0.585Å, $r_{Co4+(HS)}$=0.53Å, $r_{Fe3+(HS)}$=0.645Å, $r_{Co3+(HS)}$=0.61Å, $r_{Co2+(HS)}$=0.745Å, $r_{Co2+(HS)}$=0.780Å, all CN=6) [17] suggests that cobalt is incorporated in a lower valence than iron as was suggested in our previous paper [15].

Table 1 summarizes the composition of the samples as measured by X-ray fluorescence spectroscopy. The data suggest that all samples were B-site deficient with an A/B ratio of ~1.1 for all values of x. In all samples the major impurity was aluminum at ~0.3% on a cation basis.

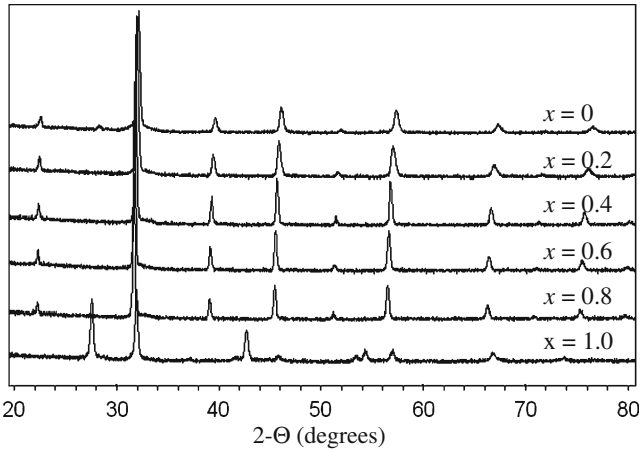

Fig. 1 Room temperature X-ray diffraction patterns for $Ba_{0.5}Sr_{0.5}Co_xFe_{1-x}O_{3-\delta}$ (x=0~1.0) calcined at 950°C in air

Figure 2 shows the microstructure of the BSCF samples sintered in air. The BSC and BSCF samples were ~90% of their theoretical densities whereas the BSF sample was ~65% of its theoretical density, as shown in Table 2. With increasing cobalt concentration, an increase in both grain size and pore size was observed. The increase in grain size with increasing x is attributed to an increase in diffusional mass transport via oxygen vacancies.

Figure 3 shows the DC conductivity of the samples measured in air. The reported data are the average of three measurements made on samples that were removed from the test chamber and re-electroded between runs. Among all of the samples, only the BSC end member (x=1.0), which has a rhombohedral rather than cubic perovskite structure, shows a continuous increase in conductivity with increasing temperature over the range measured. For the other samples ($x\leq0.8$), conductivity increases with increasing temperature from room temperature to ~400°C and then decreases with different slopes depending on composition. The decrease in conductivity with increasing temperature is most pronounced in samples with low cobalt concentrations. The maximum conductivities of 20–50 S/cm occurred around 400–500°C. In general, the trend in the electrical conductivity vs. temperature data for various Fe/Co ratios are similar to those reported by Chen et al., who reported maximum conductivities of 30–50 S/cm for BSF and BSCF samples in air at 500°C.

In Fig. 4, conductivity is plotted as a function of temperature according to Eq. 2, which is appropriate for conduction via adiabatic polaron hopping [9]:

$$\sigma = \frac{A}{T} e^{-\frac{E_a}{kT}} \tag{2}$$

where E_a is activation energy, T is temperature in Kelvin, k is Boltzmann's constant, and A is the preexponential factor that depends on the site fraction of carriers and the probability that neighboring ions are available to participate in the hopping process. The conductivity of BSC (Fig. 4(f)) is thermally activated over the entire temperature range with an activation energy of 0.21 eV. Below ~673 K, the conductivity of BSF and BSCF (Fig. 4(a–e)) is thermally activated with activation energies ranging between 0.21 eV and 0.40 eV, which are comparable to those reported by others. As points of comparison, Grunbaum et al. reported activation energies ranging from 0.28 to 0.4 eV for the cubic phase of $SrCo_{0.8}Fe_{0.2}O_{3-\delta}$ [10], and Wei et al. reported an activation energy of 0.4 eV for $Ba_{0.5}Sr_{0.5}Co_{0.8}Fe_{0.2}O_{3-\delta}$ over the temperature range 100–400°C [11]. Above 673K, the slope of the data (ln σT vs. 1/T) generally increases with increasing cobalt concentration, ranging from a negative value in BSF to a positive value in the x=0.8 sample.

The conductivity of the BSCF5582 sample was measured as a function of temperature under static pO_2 conditions ranging from 10^{-5} atm to 1 atm. In general, the features of the ln σT vs. 1/T data were similar to those shown in Fig. 4(e). In Fig. 5, log σ is plotted as a function of log pO_2 for four temperatures between 300 and 900°C. At 300°C (Fig. 5(a)), the conductivity ranges from 6–11 S/cm without a clear dependency on pO_2. At higher temperatures (Fig. 5(b–d)), the slope of log σ vs. log pO_2 is clearly positive for $pO_2\geq0.01$ atm, suggesting p-type electronic conduction. Lines showing a ¼ and 1/6 slope are shown for comparison. At $pO_2\leq0.01$ atm (Fig. 5(b–d)), the slope of the data is slightly negative with values ranging from −1/17 to−1/9.

Figure 6 summarizes the observed electrical behavior of the BSCF5582 sample investigated in this study. At low temperatures over the entire pO_2 range studied, BSCF5582 is thermally activated with E_a ranging from 0.28 eV to 0.40 eV. In this region, conductivity does not appear to be strongly dependent on pO_2. At $pO_2\geq0.01$ atm, the conductivity above 673 K is also thermally activated but with a much lower activation energy, around 0.07 eV. At $pO_2\leq0.01$ atm, conductivity increases slightly with decreasing oxygen partial pressure above 673 K. In this low-pO_2 region, the temperature dependence of conductivity changes with temperature. Above 823 K, conductivity

Table 1 Chemical composition of sintered samples as measured by X-ray fluorescence spectroscopy.

Sample	A/B	[Ba]/([Ba]+[Sr])	[Co]/([Co]+[Fe])
x=0	1.10	0.45	0
x=0.2	1.09	0.45	0.22
x=0.4	1.08	0.45	0.42
x=0.6	1.08	0.42	0.62
x=0.8	1.10	0.42	0.82
x=1.0	1.07	0.43	1.0

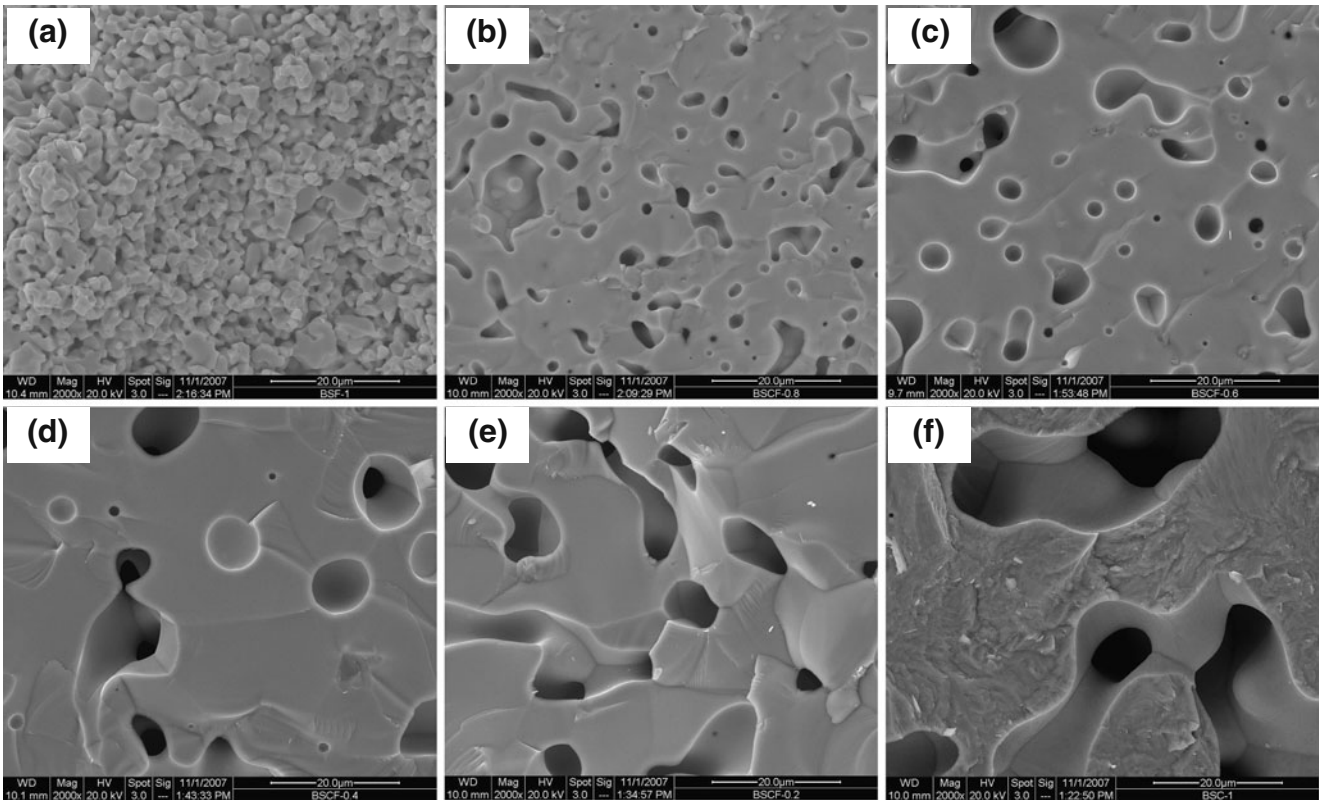

Fig. 2 Microstructures for $Ba_{0.5}Sr_{0.5}Co_xFe_{1-x}O_{3-\delta}$ (x=0~1.0) sintered at 1100°C for 5 h in air: (**a**) x=0, (**b**) x=0.2, (**c**) x=0.4, (**d**) x=0.6, (**e**) x=0.8 and (**f**) x=1.0

increases with increasing temperature and has an activation energy of around 0.2 eV. Between ~673 K and 823 K, conductivity decreases with increasing temperature.

4 Discussion

The defect chemistry of BSCF is complex. The B-site cations can adopt multiple valances and the defect concentration is sufficiently high that dilute-solution approximations may not be valid. Nevertheless, much of the observed behavior can be explained, at least qualitatively, by first assuming that the stoichiometric cubic perovskite $(Ba,Sr)^{2+}$ Fe^{4+} O_3 is the parent structure and that the substitution of trivalent cobalt on tetravalent iron sites introduces oxygen vacancies according to Eq. 3:

$$AO + (1-x)FeO_2 + \frac{x}{2}Co_2O_3 \rightarrow A_A + (1-x)Fe_{Fe} + xCo'_{Fe} + \left(3-\frac{x}{2}\right)O_O + \frac{x}{2}V_O^{\bullet\bullet} \quad (3)$$

where x is the mole fraction of Co on the B site and A denotes the mixed occupancy by Ba and Sr. As mentioned previously, the observed increase in the unit cell volume

Table 2 Lattice parameters, bulk density, mean grain size and mean pore size of $Ba_{0.5}Sr_{0.5}Co_xFe_{1-x}O_{3-\delta}$.

Sample	Lattice parameters		Bulk density (%)	Mean grain size (μm)	Mean pore size (μm)
	a (Å)	c (Å)			
x=0	3.93126 (38)	3.93126 (38)	65.5	2.7±1.2	1.5±1.3
x=0.2	3.95108 (34)	3.95108 (34)	91.1	5.5±3.3	2.6±1.8
x=0.4	3.96783 (14)	3.96783 (14)	97.6	9.8±6.0	3.6±2.5
x=0.6	3.97758 (29)	3.97758 (29)	88.6	14.1±10.5	7.8±2.4
x=0.8	3.98621 (33)	3.98621 (33)	87.6	14.8±12.3	8.4±3.8
x=1.0	9.6997(45)	13.0096 (64)	90.5	19.5±10.6	10.5±7.4

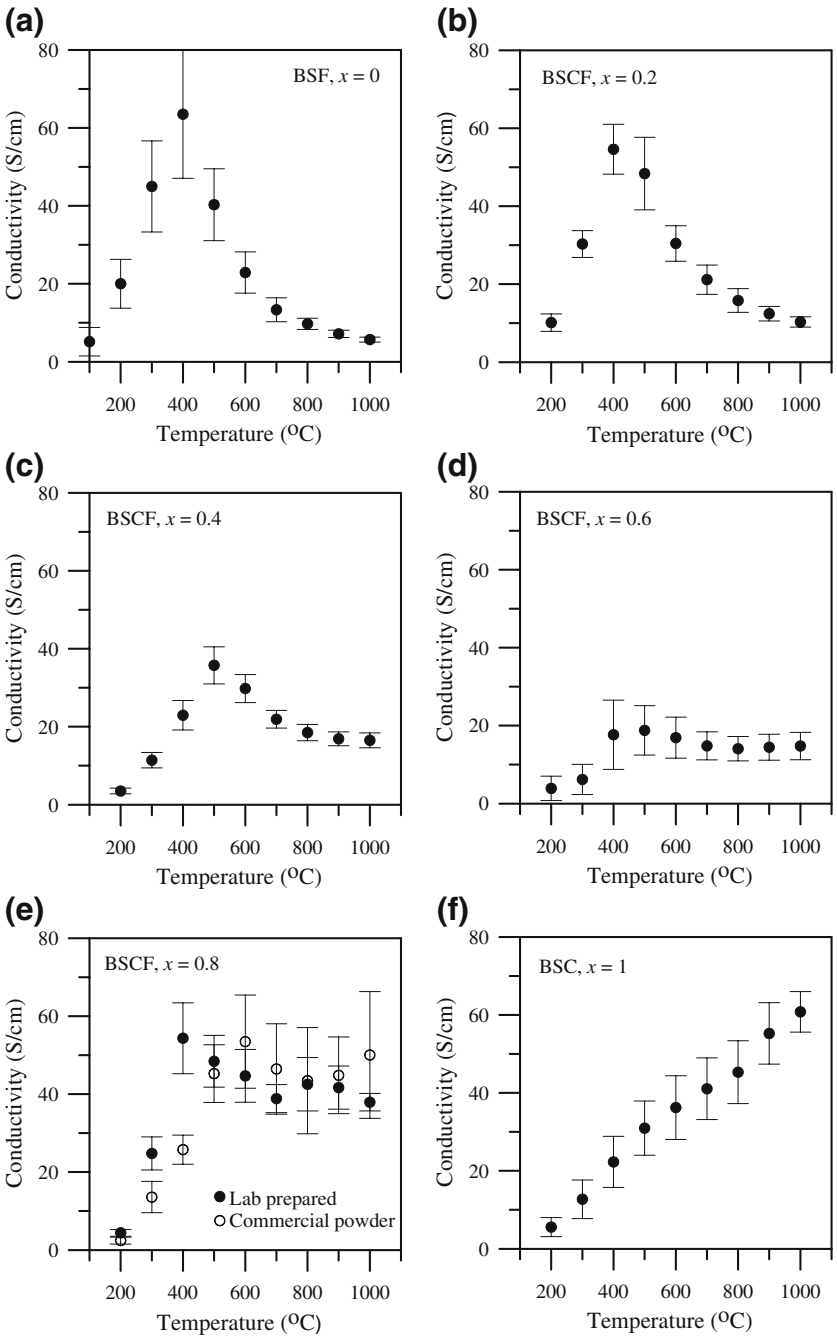

Fig. 3 DC conductivity of $Ba_{0.5}Sr_{0.5}Co_xFe_{1-x}O_{3-\delta}$ (x=0~1.0) measured in air using 4-point DC method: (**a**) BSF x=0, (**b**) x=0.2, (**c**) x=0.4, (**d**) x=0.6, (**e**) x=0.8, and (**f**) BSC, x=1.0

with increasing cobalt concentration suggests that Co is incorporated primarily in its trivalent state.

Interaction with oxygen in the atmosphere alters the concentration of the electronic charge carriers in BSCF. Under high pO_2, the filling of oxygen vacancies produces electronic holes according to Eq. 4 which has a corresponding equilibrium constant (K_{ox}):

$$\frac{1}{2}O_2(g) + V_O^{\bullet\bullet} \rightarrow O_O + 2h^{\bullet}$$
$$K_{ox} = \frac{[h]^2}{[V_O^{\bullet\bullet}]pO_2^{1/2}} = \frac{p^2}{[V_O^{\bullet\bullet}]pO_2^{1/2}} \quad (4)$$

Under low pO_2, the formation of additional oxygen vacancies produces electrons according to Eq. 5 which has a corresponding equilibrium constant (K_{red}):

$$O_O \rightarrow V_O^{\bullet\bullet} + 2e' + \frac{1}{2}O_2(g)$$
$$K_{red} = [e']^2[V_O^{\bullet\bullet}]pO_2^{1/2} \quad (5)$$

The formation of electronic carriers according to Eqs. 4 and 5 will alter the valences of the B-site cations relative to Eq. 3. The formation of holes will convert Co^{3+} to Co^{4+} whereas the formation of electrons will convert Fe^{4+} to Fe^{3+}

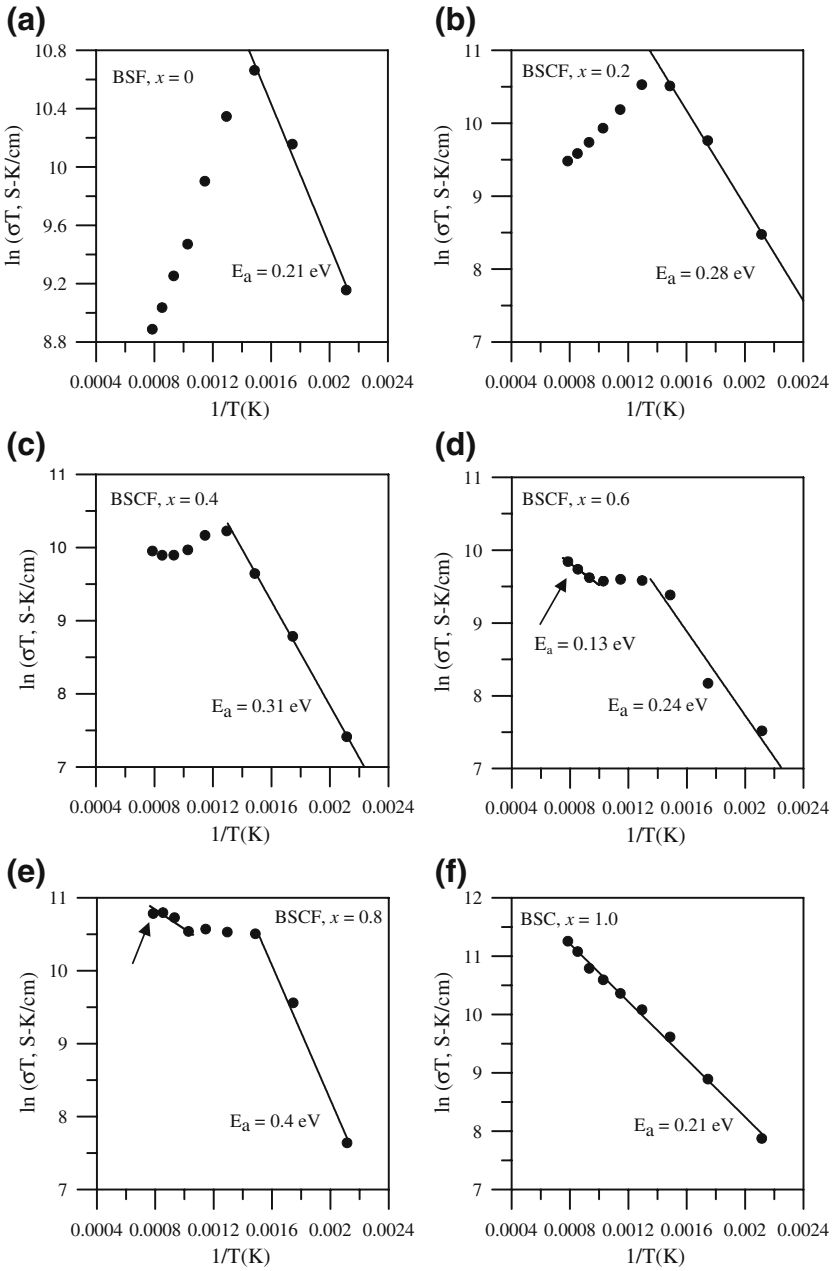

Fig. 4 Ln(σT) vs. 1/T for $Ba_{0.5}Sr_{0.5}Co_xFe_{1-x}O_{3-\delta}$ (x=0~1.0) in air: (**a**) BSF x=0, (**b**) x=0.2, (**c**) x=0.4, (**d**) x=0.6, (**e**) x=0.8, and (**f**) BSC, x=1.0

or possibly convert cobalt and iron to their divalent states. Divalent cobalt may also arise from the thermally induced charge disproportionation of Co^{3+} into Co^{4+} and Co^{2+} as reported for related oxides [9].

A general defect reaction must include species that can account for the mixed ionic and electronic conductivity of BSCF. In the absence of unambiguous information about the valences of iron and cobalt, it must also allow B-site cations to assume multiple valences depending on oxygen partial pressure and temperature. Equation 6 meets these criteria:

$$\begin{aligned} AO + (1-v-w)BO_2 + \frac{v}{2}B_2O_3 + wBO \rightarrow A_A \\ + (1-v-w-y)B_{Fe} + (v+y-z)B'_{Fe} \\ + (w+z)B''_{Fe} + \left(3-\frac{v}{2}-w-\frac{y}{2}-\frac{z}{2}\right)O_O \\ + \left(\frac{v}{2}+w+\frac{y}{2}+\frac{z}{2}\right)V_O^{\bullet\bullet} + \frac{y+z}{4}O_2(g) \end{aligned} \quad (6)$$

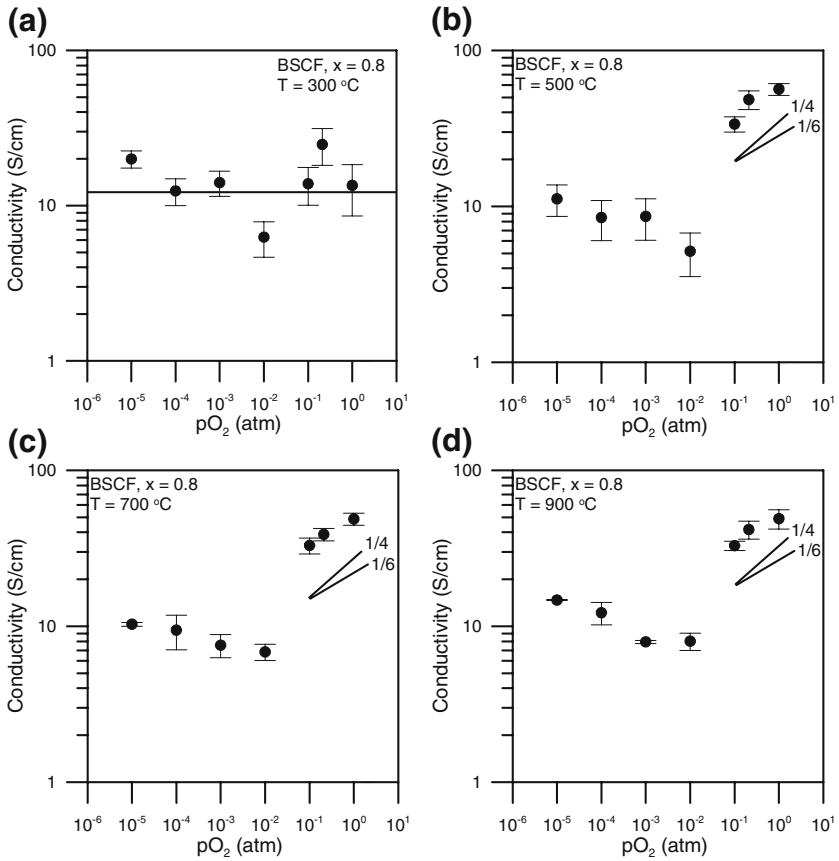

Fig. 5 Log (σ) vs. log (pO_2) for $Ba_{0.5}Sr_{0.5}Co_xFe_{1-x}O_{3-\delta}$ (x=0.8): (**a**) 300°C, (**b**) 500°C, (**c**) 700°C, and (**d**) 900°C

The variables v and w are used to identify the fraction of B-site cations in their trivalent and divalent states, respectively, at some standard state, i.e. room temperature and pO_2= 0.21 atm. The variables y and z identify the amount of B^{4+} reduced to B^{3+} and the amount of B^{3+} reduced to B^{2+}, respectively, under non-standard conditions. In other words, the values of y and z are zero at 298 K and pO_2= 0.21 atm but change with temperature and partial oxygen pressure.

Equations 4–6 provide a framework for discussing the electrical behavior of BSF and BSCF as a function of temperature and pO_2. To simplify the discussion, the ionic contribution to the total electrical conductivity is neglected, which is reasonable considering that the measured conductivities are two to three orders of magnitude higher than the ionic conductivities reported by Bucher *et al.* [6]. Because it is unlikely that equilibrium was achieved within the 10 min dwell time used in our measurements, it is important to recognize that the thermal history of the samples may influence some of the observed trends. As a point of reference, Bucher *et al.* report oxygen chemical diffusion coefficients of 10^{-6} cm^2/s for BSCF at 550°C[6]; this would imply a penetration depth of ~0.5 mm (x=$(4Dt)^{1/2}$) after 10 min whereas the shortest dimension in our samples was several millimeters.

As shown in Figs. 3 and 4, there is a marked change in the electrical behavior of BSF and BSCF at ~673 K, which

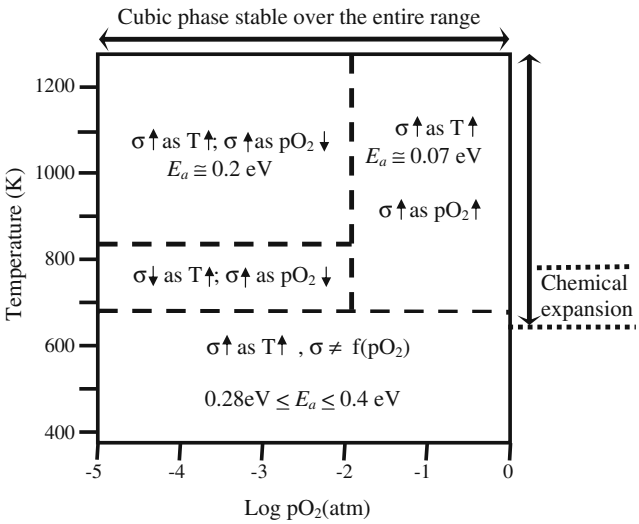

Fig. 6 Schematic diagram summarizing DC conductivity trends in $Ba_{0.5}Sr_{0.5}Co_xFe_{1-x}O_{3-\delta}$ (x=0.8) as a function of pO_2 and temperature

coincides with changes in weight loss and thermal expansion reported previously by our group [15]. Thermogravimetric analysis of the BSCF samples showed that oxygen vacancies are inactive below 673 K. According to Eqs. 4–6, this implies that carrier concentration is constant and presumably fixed by the valences of B-site cations quenched-in from higher temperatures. If conductivity is thermally activated below 673 K but carrier concentration is constant, then carrier mobility must be activated, which is indicative of a polaron hopping mechanism. P-type polaron conduction arises from hopping between B^{3+} and B^{4+} cations whereas n-type arises from hopping between B^{3+} and B^{2+}. We infer that the BSCF samples measured in air below 673 K were p-type conductors because they were quenched in air from higher temperatures where p-type behavior was observed in BSCF5582 (Fig. 5(b–d)).

When heated in air, BSCF powders undergo reversible weight loss above 673 K, which is attributed to oxygen vacancy formation. In general, the weight loss increases with increasing iron content, which suggests that it is largely associated with the reduction of iron, presumably from Fe^{4+} to Fe^{3+}. An increase in the concentration of oxygen vacancies effectively reduces the concentration of p-type carriers by producing electrons according to Eq. 5, or by increasing the values of y and z according to Eq. 6. For the x=0.6 and 0.8 samples (Fig. 4(d and e)), the activation energy observed above ~673 K results from two thermally activated processes: (1) the formation of oxygen vacancies which decreases the p-type carrier concentration and (2) the hopping of electrons between B^{3+} and B^{4+} sites. For samples with $x \leq 0.4$, the decrease in p-type carrier concentration is sufficient to result in a negative slope in the ln σT vs. 1/T graphs.

The conductivity of BSCF5582 at 300°C (Fig. 5(a)) does not show a discernable dependence on pO_2 because oxygen vacancies are inactive below 673 K. Above 673 K and at $pO_2 \geq 0.01$ atm, the conductivity increases with increasing pO_2 (Fig. 5(b–d) because oxygen vacancies are being filled and p-type carriers are being produced according to Eq. 4. According to a simple analysis of Eq. 4, the slope log(σ) vs. log pO_2 will be in the range $1/6 \leq m \leq 1/4$, depending on the electroneutrality conditions used. At $pO_2 \geq 0.1$ atm, the slope of the collected data ranges from 0.17 to 0.22 for the three different temperatures. When pO_2 is decreased from 0.1 to 0.01 atm, the conductivity drops to a value considerably lower than expected based on the high pO_2 data (Fig. 5(b–d)). A similar trend was reported by Grunbaum et al. for SCF below 973 K [10] and was attributed to the transition from a cubic perovskite structure to an orthorhombic Brownmillerite structure [4]. However, a similar phase transition has not been observed in BSCF5582 [15].

Above 673 K and at $pO_2 \leq 0.01$ atm, the conductivity of BSCF5582 increases slightly with decreasing pO_2 which suggests n-type behavior. The slopes in the log σ vs. log pO_2 graphs are much more shallow than the slope expected (m=−1/6) for a simple analysis of Eq. 5. The observed slopes may result from a broad shallow minimum in the log σ vs. log pO_2 data or from non-idealities typical of systems with high defect concentrations. While measuring the conductivity of BSCF at $pO_2 \leq 10^{-5}$ atm would be informative, it can not be accomplished with the CO/CO_2 mixtures typically used in such studies because BSCF readily reacts with CO_2.

At high temperatures (≥823 K) and low pO_2 ($pO_2 \leq$ 0.01 atm), the conductivity of BSCF is thermally activated ($E_a \cong 0.2$ eV), which may be due to hopping between B^{3+} and B^{2+} cations. However, further evidence of n-type behavior is needed. At intermediate temperatures (673–823 K) and low pO_2, conductivity decreases slightly with increasing temperature. The decrease in conductivity is not well understood, but may depend on the thermal history of the samples.

5 Conclusions

The electrical conductivity of $Ba_{0.5}Sr_{0.5}Co_{1-x}Fe_xO_{3-\delta}$ ($0 \leq x \leq 1$) was measured as a function of temperature, and the conductivity of BSCF5582 was measured as a function of pO_2 as well. Assuming that ionic conductivity is negligible, the electronic conductivity of BSCF below ~673 K in air is thermally activated ($0.2 \leq E_a \leq 0.4$ eV) and is dominated by p-type polaron hopping between B^{3+} and B^{4+} cations. Above ~673 K and $pO_2 \geq 0.01$ atm, the formation of oxygen vacancies in BSCF5582 results in a decrease in p-type carrier concentration, but conduction is still dominated by hopping between B^{3+} and B^{4+} cations. At $pO_2 \leq 0.01$ atm above ~673 K, conductivity increases with decreasing pO_2, presumably due to hopping between B^{3+} and B^{2+} cations. Above 773 K, the activation energy for conduction is ~0.2 eV.

Acknowledgements This work was supported by the New York State Foundation for Science, Technology and Innovation, NYSTAR, under contract C030093. XRF analysis of the BSCF samples was kindly provided by Dr. Joon-Hyung Lee in Kyungpook National University, South Korea.

References

1. Z. Shao, S.M. Halle, Nature **431**, 170 (2004). doi:10.1038/nature02863
2. Z. Shao, W. Yang, Y. Kong, H. Dong, J. Tong, G. Xiong, J. Membr. Sci. **172**, 177 (2000). doi:10.1016/S0376-7388(00)00337-9
3. H. Wang, Y. Cong, W.S. Wang, J. Membr. Sci. **210**, 259 (2002). doi:10.1016/S0376-7388(02)00361-7
4. S. McIntosh, J.F. Vente, W.G. Haije, D.H.A. Blank, H.J.M. Bouwmeester, Solid State Ion. **177**, 1737 (2006). doi:10.1016/j.ssi.2006.03.041

5. E. Girdauskaite, H. Ullmann, M. Al Doroukh, V. Vashook, M. Bulow, U. Guth, J. Solid State Electrochem. **11**, 469 (2007). doi:10.1007/s10008-006-0175-2
6. E. Bucher, A. Egger, P. Ried, W. Sitte, P. Holtappels, Solid State Ion. (2008). doi:10.1016/j.ssi.2008.01.089
7. Z. Chen, R. Ran, W. Zhou, Z. Shao, S. Liu, Electrochim. Acta **52**, 7343 (2007). doi:10.1016/j.electacta.2007.06.010
8. P. Zeng, Z. Chen, W. Zhou, H. Gu, Z. Shao, S. Liu, J. Membr. Sci. **291**, 148 (2007). doi:10.1016/j.memsci.2007.01.003
9. L.W. Tai, M.M. Nasrallah, H.U. Anderson, D.M. Sparlin, S.R. Sehlin, Solid State Ion. **76**, 259 (1995). doi:10.1016/0167-2738(94)00244-M
10. N. Grunbaum, L. Mogni, F. Prado, A. Caneiro, J. Solid State Chem. **177**, 2350 (2004). doi:10.1016/j.jssc.2004.03.026
11. B. Wei, Z. Lu, X. Huang, J. Miao, X. Sha, X. Xin et al., J. Eur. Ceram. Soc. **26**, 2827 (2006). doi:10.1016/j.jeurceramsoc.2005.06.047
12. L. Ge, W. Zhou, R. Ran, S. Liu, Z. Shao, W. Jin et al., J. Membr. Sci. **306**, 318 (2007). doi:10.1016/j.memsci.2007.09.004
13. L. Ge, R. Ran, K. Zhang, S. Liu, Z. Shao, J. Membr. Sci. (2008). doi:10.1016/j.memsci.2008.02.015
14. W. Zhou, R. Ran, Z. Shao, W. Zhuang, J. Jia, H. Gu et al., Acta Mater. (2008). doi:10.1016/actamat.2008.02.002
15. J. Ovenstone, J.-I. Jung, J.S. White, D.D. Edwards, S.T. Misture, J. Solid State Chem. **181**, 576 (2008). doi:10.1016/j.jssc.2008.01.010
16. S. Lee, Y. Lim, E.A. Lee, H.J. Hwang, J.-W. Moon, J. Power Sources **157**, 848 (2006). doi:10.1016/j.jpowsour.2005.12.028
17. R.D. Shannon, Acta Crystallogr. A **32**, 751 (1976). doi:10.1107/S0567739476001551